IEEE Robotics and Automation Letters (RAL) paper presented at the
2020 IEEE/RSJ International Conference on Intelligent Robots and Systems (IROS)
October 25-29, 2020, Las Vegas, NV, USA (Virtual)

The 6-DoF Implementation of the Energy-Reflection based Time Domain Passivity Approach with Preservation of Physical Coupling Behavior

Michael Panzirsch[1*] and Harsimran Singh[1*] and Christian Ott[1]
*The authors contributed equally to this work

***Abstract*— Instability due to delayed communication is one of the main challenges in the coupling of autonomous robots but also in teleoperation with applications reaching from space to tele-healthcare scenarios. The Time Domain Passivity Approach assures stability despite delay and has already been validated in teleoperation scenarios from the International Space Station. It has been improved by a method considering energy reflection of the coupling controller recently. This extension has been shown to provide better performance in terms of position tracking and transmitted impedances which promises increased transparency for a human operator. This paper presents the 6-DoF implementation of the energy-reflection based approach and of an extended gradient method which promises to maintain the physical coupling behavior despite delay. An intense experimental validation confirms the performance increase due to both methods at delays up to 600ms in the 6-DoF case.**

I. INTRODUCTION

With increased capabilities of autonomous systems and robots itself, also the diversity of applications is extended. The coupling of robotic systems is required for platooning scenarios in public transport [1], for autonomous landing in aerospace engineering [2] and also in the teleoperation of mobile robots or manipulators. Such delayed coupled network systems differ not only in the size of delay but also in the sensor equipment of the hardware. Mostly, the coupling is achieved by a controller with spring characteristics that punish a position deviation of the respective systems. Therefore, the robot poses and the computed coupling forces are exchanged via the communication channel.

In teleoperation, a human operator uses a haptic input device to control a robot in a remote environment. In the last decades, a variety of control approaches for stabilization of delayed systems based on wave variables [3] or energy based approaches as the two-layer approach [4] and Lyapunov [5] have been proposed. Among them, the Time Domain Passivity Approach (TDPA, [6]) is one of the approaches which has been most thoroughly validated for example in space applications [7], [8]. A method to conserve the force and torque arrow directions for impedance type PCs [9] was recently extended to admittance type PCs in [10] to eliminate cross-dimensional artifacts. A recent extension of the TDPA for extreme delays [11] which has been applied by the European Space Agency in the first force-feedback 6-DoF teleoperation from the International Space Station relies on the availability of measured forces but achieves most promising performance at high delay since so-called phantom forces (resulting from computed force feedback, [12]) that heavily disturb the operator at delays above 800ms are not transmitted to the operator side. At low delay, the position drift that results from this type of TDPA disturbs the performance of the teleoperation coupling. In contrast to high delays, at lower delay, the phantom forces resulting from computed force feedback do not deteriorate the transparency in a critical way but can even provide the operator with additional information on the robot dynamics. Therefore, a different approach was developed that considers the energy reflection of the coupling controller (TDPA-ER, [13]). Since this approach does not require the measurement of external forces, is free of position drift and has been shown to provide better position tracking and higher transmitted impedances to the operator, it is currently under review for the first IEEE Standard for delayed teleoperation.

In contrast to the original TDPA [14] which passivity controls the two directions of energy flow between the coupled systems separately, the TDPA-ER considers a common energy storage which represents the desired potential energy of the coupling controller and which is charged up from both energy flow directions. The energy exit from this storage is then limited according to the passivity condition by passivity controllers (PC) that vary the output forces with an adaptive damping (impedance-type PC). This approach was later combined with a communication deadband approach that promises to maintain sufficient performance in case of limited link data budget [15].

In teleoperation, the delay itself diminishes the transparency since the force feedback does not arrive instantaneously after the operator's motion. As a result, when the operator moves out of a wall contact, he or she receives a delayed force of the contact, even when the pose of the input device refers already to a future robot pose without contact. This issue was tackled by the authors of [16] for the original TDPA based on an observer-based gradient method (OBG) which aims to preserve the physical coupling behavior despite communication delay. Since this combination cannot prevent position drift, an extended OBG was later integrated into the TDPA-ER [17].

In this paper, we extend the TDPA-ER as well as the corresponding OBG of [17] to the 6 degree of freedom (DoF)

[1]M. Panzirsch, H. Singh and C. Ott are with the Institute of Robotics and Mechatronics in the German Aerospace Center (DLR), 82234 Wessling, Germany. michael.panzirsch@dlr.de

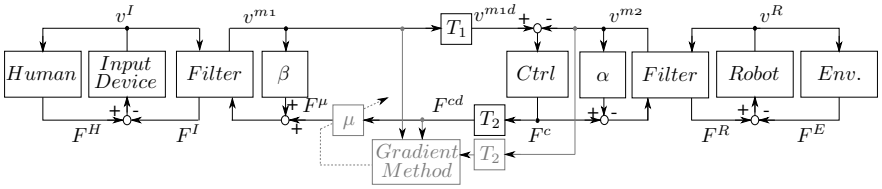

Fig. 1: Signal Flow Diagram of a Delayed Coupled Network System

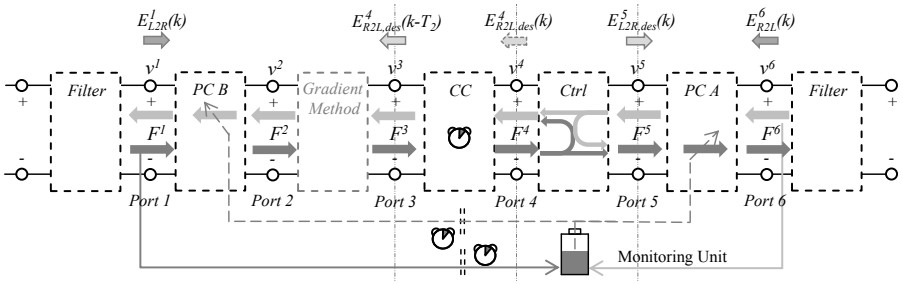

Fig. 2: Network Representation of a Delayed Coupled Network System

case. The TDPA-ER as well as the OBG method in general have so far only been presented in 1-DoF analyses and a purely translational 3-DoF analysis [15]. Furthermore, an extension of the OBG to prevent force jumps is introduced.

II. FUNDAMENTALS

A. Energy Reflection-Based TDPA

This section reviews the principles of energy observation and the energy reflection-based TDPA (TDPA-ER). The signal flow diagram in Fig. 1 presents a teleoperation control loop with a controller (Ctrl) which couples a remote robot (R) with a haptic input device (I). A position reference v^{m1} is sent to the robot on the right side of the communication channel (CC) and the computed controller force F^c which coordinates the coupling of the devices is fed back to the input device on the left side of the CC. The adaptive dampings α and β represent impedance type passivity controllers (PC) that assure the stability of the control loop despite delayed communication (T_1 and T_2). The PCs vary the forces that are sent to the input device and robot. Two passive filters [14] are integrated that smooth the output force of the PCs which have high-frequency disturbances due to the PC action. Fig. 2 shows the network representation of the respective control setup. The PCs of the TDPA-ER assure the passivity of the 2-port including CC and Ctrl. The Ctrl is represented by an energy storage (monitoring unit) since the controller's spring component resembles a potential energy reservoir. The energy monitoring unit is charged up by the energy input from the input device at port 1 in left to right direction (L2R) E^1_{L2R} and from the robot in right to left direction (R2L) at port 6 E^6_{R2L}. The energy which may exit the storage element in L2R direction at port 5 $E^5_{L2R,des}(k)$ and port 2 in R2L direction $E^4_{R2L,des}(k-T_2)$ in time step k is limited according to the energy content of the monitoring unit. The PC A can directly assure the respective energy dissipation whereas the PC B has to consider the delayed desired output energy $E^4_{R2L,des}(k-T_2)$ at port 2. As discussed in [15], it is important to consider the transmission of energies $E^4_{R2L,des}(k-T_2)$ instead of powers $P^4_{R2L,des}(k-T_2)$ (compare [13]) in case of communication links with high packet loss.

The power or energy flow in the system can be determined from the power-correlated signals at the ports i of a network subsystem: $P^i(k) = v^i(k)F^i(k)$. The direction of power flow can be analyzed from the sign of the power:

$$P^i_{L2R}(k) = \begin{cases} 0, & \text{if } P^i(k) < 0 \\ P^i(k), & \text{if } P^i(k) > 0, \end{cases} \tag{1}$$

$$P^i_{R2L}(k) = \begin{cases} 0, & \text{if } P^i(k) > 0 \\ -P^i(k), & \text{if } P^i(k) < 0, \end{cases} \tag{2}$$

and via integration, the energies can be calculated: $E^i_{L2R}(k) = T_s \sum_{j=0}^{k} P^i_{L2R}(j)$ and $E^i_{R2L}(k) = T_s \sum_{j=0}^{k} P^i_{R2L}(j)$, with the sampling time T_s. The energy monitoring unit considers the energy storage E_{st} which is charged up from port 1 and 6:

$$\begin{aligned} E_{st}(k) = E_{st}(k-1) + E^1_{L2R}(k-T_1) - \\ E^1_{L2R}(k-T_1-1) + E^6_{R2L}(k) - E^6_{R2L}(k-1) - \\ P^4_{R2L,des}(k-1)T_s - P^5_{L2R,des}(k-1)T_s. \end{aligned} \tag{3}$$

$P^4_{R2L,des}$ and $P^5_{L2R,des}$ are zero in the first time step and will be defined in the next paragraph.

To calculate the desired limited power output $P^5_{L2R,des}$ and $P^4_{R2L,des}$, the actual output power $P^{act}_{out}(k)$ of the energy storage element has to be determined:

$$P^{act}_{out}(k) = P^4_{R2L}(k) + P^5_{L2R}(k). \tag{4}$$

The limited power output results in:

$$P^4_{R2L,des}(k) = \begin{cases} P^4_{R2L}(k) & +P_{exc}(k)\frac{P^4_{R2L}(k)}{P^{act}_{out}(k)}, \\ & \text{if } \frac{E_{st}(k)}{T_s} < P^{act}_{out}(k) \\ P^4_{R2L}(k), & \text{if } \frac{E_{st}(k)}{T_s} > P^{act}_{out}(k), \end{cases} \tag{5}$$

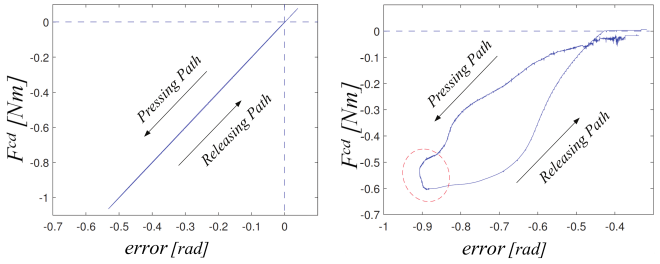

(a) $T_{rt} = 0ms$ (b) $T_{rt} = 200ms$

Fig. 3: Experimental result for error vs force.
Source: Adapted from [16]

where the excessive power $P_{exc}(k)$ that has to be dissipated in the current time step is

$$P_{exc}(k) = E_{st}(k)/T_s - P_{out}^{act}(k). \tag{6}$$

The power $P_{L2R,des}^{5}(k)$ is calculated analogous to (5) with P_{L2R}^{5}instead of P_{R2L}^{4}.

The energies $W_{obs}^{PCA}(k)$ and $W_{obs}^{PCB}(k)$ have to be dissipated by the PCs:

$$\begin{aligned} W_{obs}^{PCA}(k) =& E_{L2R,des}^{5}(k) - \sum_{j=0}^{k} P_{L2R}^{5}(j)T_s \\ & - W_{diss}^{PCA}(k-1), \end{aligned} \tag{7}$$

$$\begin{aligned} W_{obs}^{PCB}(k) =& E_{R2L,des}^{4}(k-T_2) - \sum_{j=0}^{k} P_{R2L}^{2}(j)T_s \\ & - W_{diss}^{PCB}(k-1). \end{aligned} \tag{8}$$

W_{diss} is the energy that was already dissipated by the respective PC. The functionality of the PC is described in Section III-A. Then, the 2-port passivity condition

$$E_{R2L}^{1}(k) + E_{L2R}^{6}(k) \leq E_{L2R}^{1}(k) + E_{R2L}^{6}(k) \tag{9}$$

is fulfilled.

B. Gradient method to preserve physical coupling behavior

In this section, the passive filters are neglected such that the delayed robot pose is considered. The OBG method, when implemented alongside TDPA, reduces the high frequency force vibrations generated by the impedance type PC on the operator side. An observer is implemented at port 2 on the operator side, which at every sample detects whether the rate of change of error between the input device and robot pose increases ($\dot{\bar{e}}^I(k) > 0 \& F^{cd}(k) > 0$ or $\dot{\bar{e}}^I(k) < 0 \& F^{cd}(k) < 0$) or decreases ($\dot{\bar{e}}^I(k) \leq 0 \& F^{cd}(k) > 0$ or $\dot{\bar{e}}^I(k) \geq 0 \& F^{cd}(k) < 0$), while the user maintains robot-environment contact, where $\dot{\bar{e}}^I(k) = v^I(k) - v^R(k-T_2)$, $v^I(k)$ is the input device velocity, $v^R(k-T_2)$ is the delayed robot velocity, and $F^{cd}(k) = F^c(k-T_2)$ is the delayed feedback force from the robot. Due to communication delay, the feedback force increases even when the user tends to move out of contact with the remote environment, which might cause misinterpretation regarding the environment's property. Alternately it can also be said that due to delay in the communication channel, the gradient ($\dot{F}^{cd}(k)/\dot{\bar{e}}^I(k)$) goes negative, when the user is moving out of contact with the environment. This introduces additional E_{R2L}^{3} energy which then has to be dissipated by the PC. However, for systems with no communication delay, this gradient is always positive. This occurrence can be clearly observed from the error-force graph in Fig. 3. A controller with adaptive gain is implemented which makes sure that the gradient is positive. The controller ensures that the magnitude of force after gradient controller $F^{\mu}(k)$ is equal to the magnitude of delayed feedback force ($|F^{\mu}(k)| = |F^{cd}(k)|$) during pressing path ($|v^I(k)| - |v^R(k-T_2)| > 0$), and $|F^{\mu}(k)| \leq |F^{cd}(k)|$ during releasing path ($|v^I(k)| - |v^R(k-T_2)| \leq 0$). Thus, the delayed feedback force is rectified by removing the undesired increase in force due to the time delay. During releasing path, $F^{\mu}(k)$ reaches 0 before $F^{cd}(k)$ and holds that value. As a result of this, there is a dead-band where the user has the perception of no-contact even though the robot is in contact with the remote environment. Therefore, a local virtual coupling depending on $\bar{e}^I$ is adapted on the operator side during the releasing path. The stiffness gain of this coupling is $F^{\mu}(k-1)/\bar{e}^I(k-1)$ and is computed at every sample of releasing path. The controller is modified based on the computed stiffness of the local coupling, which makes sure that the force during releasing path gradually decreases to 0 when $\bar{e}^I = 0$.

$$\mu = \begin{cases} Pressing: & 1, \\ Releasing: & \\ \quad \frac{\bar{e}^I(k)F^{\mu}(k-1)}{F^{cd}(k)\bar{e}^I(k-1)}, & \text{if } F^{\mu}(k) \leq F^{cd}(k) \\ \quad 1, & \text{if } F^{\mu}(k) > F^{cd}(k) \\ No\ Contact: & 0. \end{cases} \tag{10}$$

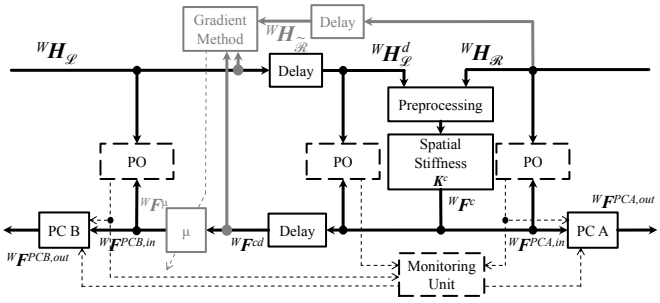

Fig. 4: Signal Flow of the 6-DoF Control Structure

III. 6-DoF FORMULATION OF TDPA-ER AND OBG

In the following, ${}^{i}\boldsymbol{H}_{j}$ is the homogenous transform $\boldsymbol{H}$ describing frame j in frame i which transforms a vector from frame j into frame i and ${}^{q}z^{e}$ is a vector or matrix z of e (e.g. device) described in frame q.

Fig. 4 presents the signal flow diagram of the 6-DoF TDPA-ER structure. The gray parts relate to the OBG and will be described later. A passive spatial spring [18] is applied as the coupling controller. ${}^{W}\boldsymbol{H}_{\mathscr{L}}$ and ${}^{W}\boldsymbol{H}_{\mathscr{R}}$ are the poses of the left and right side devices respectively. If the passive filters of [14] are applied, the left side input

${}^W\boldsymbol{H}_{\mathscr{L}} = {}^W\boldsymbol{H}_{m1}$ equals to the pose of the operator side filter's mass $m1$ and the right side input ${}^W\boldsymbol{H}_{\mathscr{R}} = {}^W\boldsymbol{H}_{m2}$ equals to the pose of the robot side filter's mass $m2$. The passive filters consist of a virtual object with an inertia mj and moment of inertia $Mj_{x,y,z}$, of the stiffness $\boldsymbol{K}^{mj}$ and damping $\boldsymbol{B}^{mj}$ coupling the mass with the respective device j and an additional local damping $\boldsymbol{B}^{l,mj}$ on the mass.

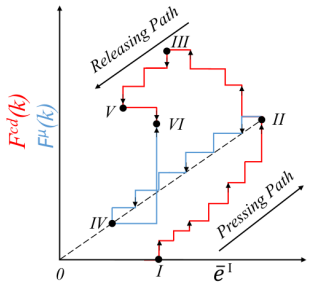

Fig. 5: Schematic with force jumps

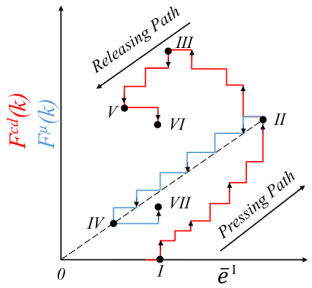

Fig. 6: Schematic with smooth force transitions

A. Energy Reflection-Based TDPA

The TDPA-ER requires three 6-DoF passivity observers at port 2, 4 and 5. Here, the control structure is implemented in a way that all wrenches and twists are defined in the world frame W such that all powers are uniformly calculated in W. With the generalized twist ${}^W v_d^i$ and the generalized wrench ${}^W F_d^i$ in DoF $d \in \mathbb{N}$, $d \in [1,6]$, the power ${}^W P_d^i$ at port i can be measured: ${}^W P_d^i(k) = {}^W v_d^i(k) {}^W F_d^i(k)$. $W_{obs,d}^{PCA}(k)$ and $W_{obs,d}^{PCB}(k)$ can be calculated analogous to (7) and (8). Both 6-DoF impedance type passivity controllers $PC\ A$ and $PC\ B$ vary the output wrench ${}^W F_d^{PCA,out}(k) = {}^W F_d^6(k)$ and ${}^W F_d^{PCB,out}(k) = {}^W F_d^1(k)$ with a 6-DoF damping vector α ($PC\ A$) or β ($PC\ B$) respectively:

$$ {}^W F_d^{PCA,out}(k) = {}^W F_d^5(k) + \alpha_d(k) {}^W v_d^5(k), \text{ with} \tag{11} $$

$$ \alpha_d(k) = \begin{cases} \frac{W_{obs,d}^{PCA}(k)}{T_s {}^W v_d^{5\,2}(k)} & \text{if } W_{obs,d}^{PCA}(k) < 0 \\ 0 & \text{if } W_{obs,d}^{PCA}(k) \geq 0, \end{cases} \tag{12} $$

where T_s is the sampling rate. The same holds analogous for $PC\ B$:

$$ {}^W F_d^{PCB,out}(k) = {}^W F_d^2(k) + \beta_d(k) {}^W v_d^2(k), \text{ with} \tag{13} $$

$$ \beta_d(k) = \begin{cases} \frac{W_{obs,d}^{PCB}(k)}{T_s {}^W v_d^{2\,2}(k)} & \text{if } W_{obs,d}^{PCB}(k) < 0 \\ 0 & \text{if } W_{obs,d}^{PCB}(k) \geq 0. \end{cases} \tag{14} $$

Another mathematically reasonable option of 6-DoF dissipation is to consider the sum of energy in translations and rotations in the passivity control. Then, the length of the force and torque vector can be varied by the passivity controller. Still, especially at high delay this method might lead to unexpected behavior since, (although mathematically correct) from a physical perspective, due to the summation of energies, the knowledge in which DoF energy has to be dissipated is lost. The respective analysis remains for future work.

B. Extension of OBG Method to prevent force jumps

In the following, $\tilde{\mathscr{R}}$ refers to the delayed robot information on the operator side. Whereas, the extension of the OBG is straightforward for the translations, the computation of the pose error in the orientation requires adaptations. To determine the error ${}^W\bar{\boldsymbol{H}}_W$ defined in the world frame W, the operator side robot reference pose ${}^W\boldsymbol{H}_{\tilde{\mathscr{R}}^*}$ has to be determined as

$$ {}^W\boldsymbol{H}_{\tilde{\mathscr{R}}^*}(k) = ({}^W\boldsymbol{H}_{\mathscr{L}}(0) {}^W\boldsymbol{H}_{\mathscr{L}}{}^1(k))\ {}^1{}^W\boldsymbol{H}_{\tilde{\mathscr{R}}}(0), \tag{15} $$

with the initial operator side pose ${}^W\boldsymbol{H}_{\mathscr{L}}(0)$ and the delayed pose ${}^W\boldsymbol{H}_{\tilde{\mathscr{R}}}(0)$ of the right side mass or robot. The error ${}^W\bar{\boldsymbol{H}}_W$ can then be found as

$$ {}^W\bar{\boldsymbol{H}}_W(k) = {}^W\boldsymbol{H}_{\tilde{\mathscr{R}}}(k) {}^{\tilde{\mathscr{R}}^*}\boldsymbol{H}_{\tilde{\mathscr{R}}}{}^1(k), \text{ with} \tag{16} $$

$$ {}^{\tilde{\mathscr{R}}^*}\boldsymbol{H}_{\tilde{\mathscr{R}}}(k) = {}^W\boldsymbol{H}_{\mathscr{L}}{}^1(k) {}^W\boldsymbol{H}_{\tilde{\mathscr{R}}}(k). \tag{17} $$

The translational error ${}^W\bar{\boldsymbol{x}}$ can be directly extracted from ${}^W\bar{\boldsymbol{H}}_W$. The rotational error is calculated as $\bar{\Theta}{}^W\bar{\boldsymbol{p}}$ with the angle $\bar{\Theta}$ and the axis ${}^W\bar{\boldsymbol{p}}$ of the angle-axis representation which can be found via the Rodriguez equation from ${}^W\bar{\boldsymbol{R}}_W$, such that the operator side error vector ${}^W\bar{e}^I$ becomes: ${}^W\bar{e}^I = \left[{}^W\bar{\boldsymbol{x}}, \bar{\Theta}{}^W\bar{\boldsymbol{p}}\right]$. The integration of the 6-DoF OBG into the TDPA-ER structure is depicted in the gray parts of Fig. 4.

Algorithm 1: OBG without force jumps

```
if Pressing Path then
    μ_d(k) = (W F_d^μ(k 1) + ΔW F_d^cd(k)) / (W F_d^cd(k))
    if |W F_d^cd(k)| < |W F_d^cd(k−1)| then
        μ_d(k) = (W F_d^μ(k 1) ΔW F_d^cd(k)) / (W F_d^cd(k))
    if |W F_d^μ(k)| ≥ |W F_d^cd(k)| then
        μ_d(k) = 1
else
    if |W F_d^μ(k−1)| ≤ |W F_d^cd(k)| then
        μ_d(k) = (ē_d^I(k) W F_d^μ(k 1)) / (W F_d^cd(k) ē_d^I(k 1))
    else
        μ_d(k) = 1
```

The OBG described in Section II-B might experience force jumps, e.g., when the user is performing a manipulation task while the remote robot is in contact with the remote environment. According to (10) in every DoF, $|{}^W\boldsymbol{F}_d^{\mu}(k)| \leq |{}^W\boldsymbol{F}_d^{cd}(k)|$ during every sample of the releasing path due to the local virtual coupling, while $|{}^W\boldsymbol{F}_d^{\mu}(k)| = |{}^W\boldsymbol{F}_d^{cd}(k)|$ during every sample of the pressing path. Thus, if there is a back and forth motion commanded by the user, which toggles the controller's state from releasing to pressing, then this might result in discontinuous force jumps. Assume that at the end of any random releasing path, the force after the gradient controller $|{}^W\boldsymbol{F}_d^{\mu}(k)|$ and the delayed force feedback $|{}^W\boldsymbol{F}_d^{cd}(k)|$ is at states IV and V, as labeled on the error vs. force schematic in Figs. 5 and 6. Thereon, when $|{}^W\boldsymbol{F}_d^{cd}(k)|$ moves to state VI during the first sample of the consecutive pressing path, ${}^W\boldsymbol{F}_d^{\mu}(k)$ jumps from IV to VI due to $\mu_d = 1$ in (10), Fig. 5. To counter such discontinuous force jumps when switching from releasing

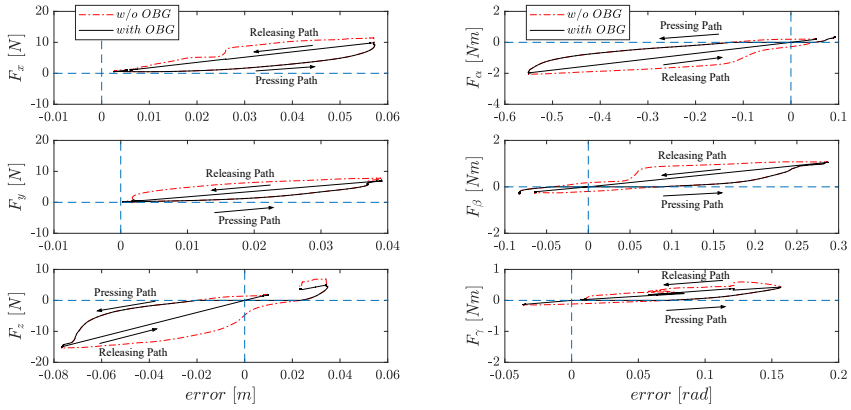

(a) Forces (b) Torques

Fig. 7: 6-DoF experiment: OBG Method at 200ms RTD

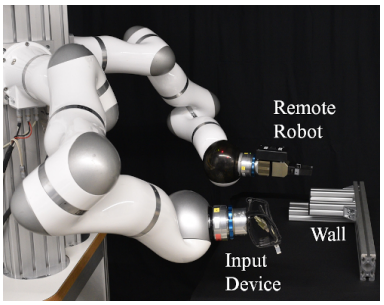

Fig. 8: Experimental Setup

to pressing path, the OBG is modified (Algorithm 1) to gradually increase or decrease the force during every sample of the pressing path such that ${}^W\dot{\boldsymbol{F}}_d^{\mu}(k) = {}^W\dot{\boldsymbol{F}}_d^{cd}(k)$, as long as $|{}^W\boldsymbol{F}_d^{\mu}(k)| < |{}^W\boldsymbol{F}_d^{cd}(k)|$, else ${}^W\boldsymbol{F}_d^{\mu}(k) = {}^W\boldsymbol{F}_d^{cd}(k)$. This is shown in the schematics of Fig. 6, where during the first sample of the consecutive pressing path when ${}^W\boldsymbol{F}_d^{cd}(k)$ moves from state V to VI, $|{}^W\boldsymbol{F}_d^{\mu}(k)|$ only moves from state IV to VII, thereby showing a smoother force transition instead of the previously observed force jump. There might be instances where this adaptation would result in negative gradient during pressing path due to time delay, which is allowed as this mainly contributes to E^3_{L2R}. Since $|{}^W\boldsymbol{F}_d^{\mu}(k)| < |{}^W\boldsymbol{F}_d^{cd}(k)|$ at all instances, the output energy at the operator side E^2_{R2L} observed with ${}^W\boldsymbol{v}^I{}^W\boldsymbol{F}_d^{\mu}$ as the supply rate will always be less than E^3_{R2L}. Therefore, the impedance PC will always end up dissipating less energy than without OBG. Figure 7a and Fig. 7b show experimental data of error vs wrench for all 6-DoFs using DLR light weight robots (LWR, see Fig. 8) as input device and remote robot with a 200ms roundtrip-delay (RTD). During the pressing path, the forces and torques follow the delayed computed feedback force. However, during the releasing path the wrenches are computed based on a local coupling spring of variable stiffness. Therefore, it can be observed that with the modified OBG (i) there are no unwanted force jumps, (ii) ${}^W\boldsymbol{F}_d^{\mu}(k) \leq {}^W\boldsymbol{F}_d^{cd}(k)$ at all instances, which means that the impedance PC would be triggered less often, and (iii) there is no dead-band during the releasing path, thereby preserving the physical coupling behavior of a bilateral teleoperation setup.

IV. EXPERIMENTS

The following experiments were performed with two DLR light weight robots (LWR) and the control software of operator and robot side was executed on one rtlinux system. The simulated delays were chosen as constant values for ease of analysis, but the TDPA is known to be robust to variable delay, packet loss and jitter. The control parameters which were tuned to the subjectively rated best performance are presented in Table I.

Translational Stiffness in $\boldsymbol{K}^c$ and $\boldsymbol{K}^{mj}$	600 N/m
Rotational Stiffness in $\boldsymbol{K}^c$ and $\boldsymbol{K}^{mj}$	20 Nm/rad
Translational Damping in $\boldsymbol{B}^{l,D}$	6.2 Ns/m
Rotational Damping in $\boldsymbol{B}^{l,D}$	0.36 Nms/rad
Inertia mj	0.01 kg
Moment of Inertia $Mj_{x,y,z}$	0.01 m^2kg
Translational Damping in $\boldsymbol{B}^{mj}$	4 Ns/m
Rotational Damping in $\boldsymbol{B}^{mj}$	0.01 Nms/rad
Translational Damping in $\boldsymbol{B}^{l,mj}$	4 Ns/m
Rotational Damping in $\boldsymbol{B}^{l,mj}$	0.5 Nms/rad

TABLE I: Controller Parametrization

A. Energy Reflection-Based TDPA

The first set of experiments evaluates the performance of the TDPA-ER without OBG. Fig. 9 to Fig. 12 evaluate the system performance at 100ms roundtrip-delay. The pose plot in Fig. 9 shows a free motion at $t = [10s - 20s]$ and a wall contact of the robot in z-direction at $t = [20s - 25s]$ which is marked with a shaded area. After another free motion phase, a wall contact in z- and β-direction is presented at $t = [30s - 38s]$. Although the input device and robot are coupled via two 6-DoF passive filters, the position tracking shows good performance and no position drift appears. The wrench plots of Fig. 10 and Fig. 11 present the spring wrench ${}^W\boldsymbol{F}^c$, the dissipation effect of the PCs ${}^W\boldsymbol{F}^{PC,out}$ and the filter output wrenches ${}^W\boldsymbol{F}^I$ and ${}^W\boldsymbol{F}^R$. The operator side $PC\ B$ dissipates more often than the robot side $PC\ A$. The passive filters clearly smooth the high frequency disturbances in the PC output wrench, but the filtered wrenches ${}^W\boldsymbol{F}^I$ and ${}^W\boldsymbol{F}^R$ follow well the delayed ${}^W\boldsymbol{F}^{cd}$ and undelayed spring wrench ${}^W\boldsymbol{F}^c$ respectively. Since the energy E_{2port} which results from the difference of input and output energies of the 2-port subsystem between port 1 and 6

$$E_{2port}(k) = E^1_{L2R}(k) - E^1_{R2L}(k) + E^6_{R2L}(k) - E^6_{L2R}(k) \tag{18}$$

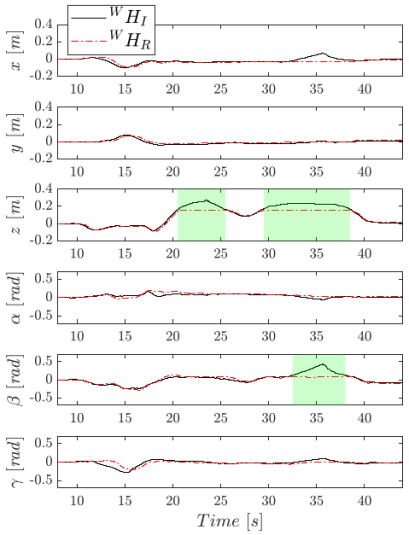

Fig. 9: Pose of Input Device and Robot at 100ms RTD (w/o OBG)

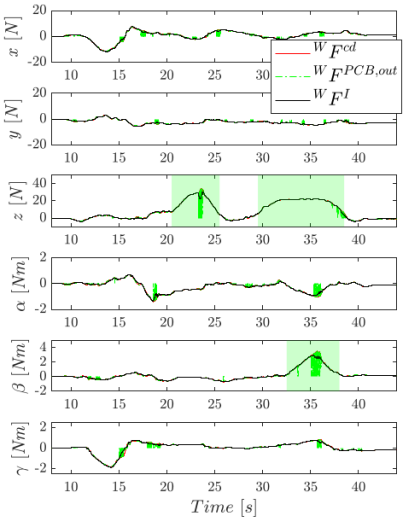

Fig. 10: Wrench on Operator Side at 100ms RTD (w/o OBG)

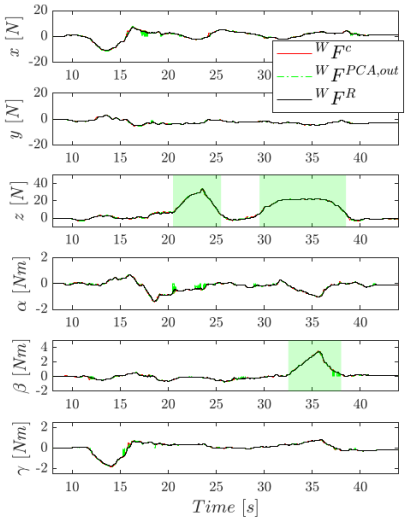

Fig. 11: Wrench on Remote Side at 100ms RTD (w/o OBG)

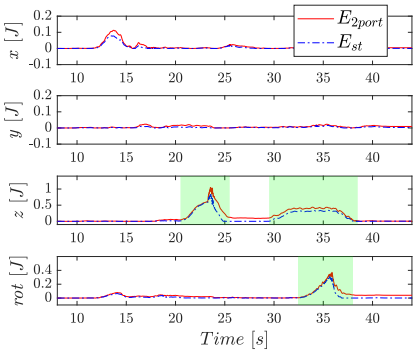

Fig. 12: Passivity Conf. of 2-port at 100ms RTD (w/o OBG)

in Fig. 12 is always positive, the 2-port passivity is confirmed. E_{st} is the energy which is available in the energy monitoring unit.

An analogous experiment is repeated for 600ms RTD in Fig. 13 to Fig. 16. A 600ms roundtrip-delay corresponds to a communication link with geostationary relay satellite. As visible from the pose plot in Fig. 13, a pure translational wall contact at $t = [15s - 20s]$ and a combined wall contact in z- and β-direction were performed at $t = [24s - 31s]$. Despite high delay and passivity control, the filtered wrench resulting from the wall contacts is well perceivable on the operator side ${}^W\boldsymbol{F}^I$. The energy E_{2port} in Fig. 16 again confirms the passivity of the delayed 2-port. Due to the delay effect, the operator cannot well perceive when the robot stops applying a force after the wall contact. Therefore, the operator moves away from the wall although he wants to keep the contact (see Fig. 13, $t = [20s - 24s]$). When the operator releases the wall contact in β-direction, the delayed torque leads to an overshoot into the opposite direction. Also, oscillations appear during free motion and wall contact (compare y-Force plot in Fig. 14, $t = [10s - 20s]$) which clearly reduces the operation performance. These negative properties can be reduced when an additional damping is introduced or the coupling stiffness is reduced. The next section shows that no oscillations appear in case of the observer-based gradient method without adaptation of coupling controller parametrization.

B. Observer-Based Gradient Method

The following experiments were performed with OBG. The preceding experiment at 600ms RTD is repeated with OBG (see Fig. 17 to Fig. 20). Fig. 17 depicts the high performance position tracking despite high delay and passivity control. A wall contact in z-direction at $t = [12s - 18s]$ is followed by a wall contact in β-direction at $t = [23s - 32s]$. No oscillations and no position drift appear and the input device ${}^W\boldsymbol{F}^I$ as well as the robot wrench ${}^W\boldsymbol{F}^R$ are of promising quality with respect to force tracking and jitter. The passive filters smooth the passivity controlled signal well and Fig. 20 confirms the 2-port passivity.

The comparison of TDPA-ER without and with OBG in Fig. 21a and Fig. 21b hints why the OBG reduces oscillations in the coupling. During the two fast wall contacts in z-direction (at $t = [22s - 24s]$ and $t = [35s - 36.5s]$), the input device was grasped loosely. In case of OBG (compare Fig. 21b), when the user moves the input device in free space towards the wall (at $t = [33.5s]$), the OBG output wrench ${}^W\boldsymbol{F}^\mu$ precisely follows the delayed computed wrench ${}^W\boldsymbol{F}^{cd}$ because

$$\mu_d = \frac{{}^W F_d^\mu(k-1) + \Delta {}^W F_d^{cd}(k)}{{}^W F_d^{cd}(k)} \tag{19}$$

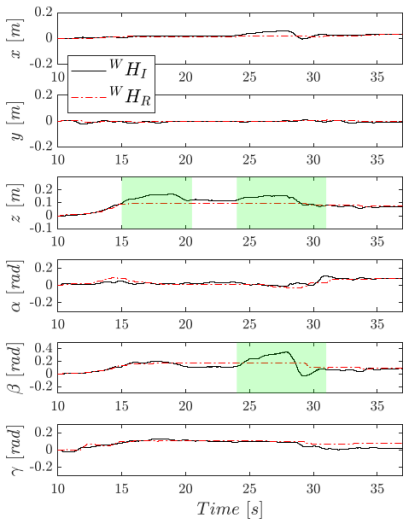

Fig. 13: Pose of Input Device and Robot at 600ms RTD (w/o OBG)

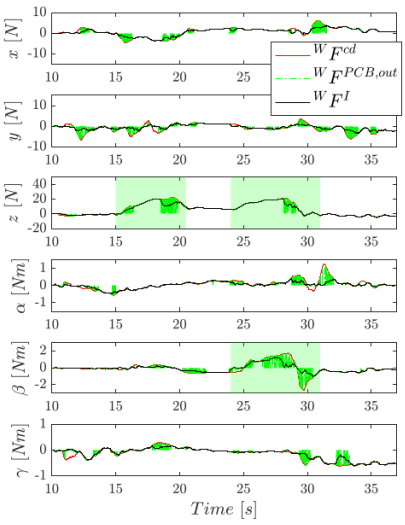

Fig. 14: Wrench on Operator Side at 600ms RTD (w/o OBG)

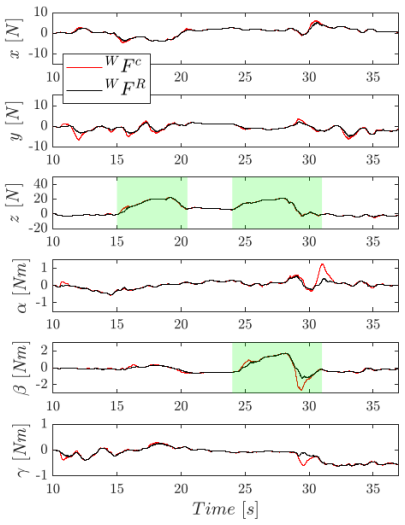

Fig. 15: Wrench on Remote Side at 600ms RTD (w/o OBG)

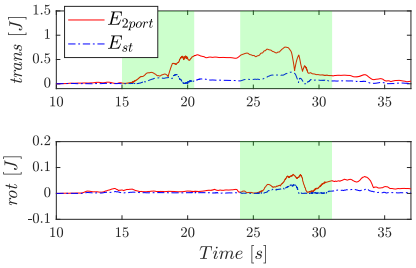

Fig. 16: Passivity Conf. of 2-port at 600ms RTD (w/o OBG)

due to ${}^{W}\dot{\boldsymbol{F}}^{cd}(k) > 0$, as described in Pressing Path of Algorithm 1. When the user starts to break the robot-environment contact (at $t = [36s]$), ${}^{W}\boldsymbol{F}^{\mu}$ drops much earlier than ${}^{W}\boldsymbol{F}^{cd}$, due to

$$\mu_d = \frac{\bar{e}_d^I(k)\,{}^{W}F_d^{\mu}(k-1)}{{}^{W}F_d^{cd}(k)\bar{e}_d^I(k-1)} \tag{20}$$

as described in Releasing Path of Algorithm 1, to imitate the desired physical coupling behavior during the release path. Therefore, the loosely grasped input device stops earlier than in the case without OBG and is zero, when input device and delayed robot pose match at $t = 37s$ close to the wall position. In contrast, in Fig. 21a, the input device receives an accelerating force even long after the user breaks robot-environment contact and the input device and delayed robot pose have crossed each other at $t = 24s$, which leads to a large overshoot of the input device. Since this effect repeats for each spring deflection sequence, the input device and robot poses oscillate in case of deactivated OBG.

V. CONCLUSIONS

This paper presented the 6-Dof implementation of TDPA-ER and observer-based gradient method. Also, the OBG was adapted to prevent force jumps during contacts. The experiments underlined the beneficial properties of both methods also in the 6-DoF case. Due to TDPA-ER, no position drift appears and despite dissipation by the PCs the force feedback is of sufficient quality with respect to force tracking and jitter. The TDPA-ER requires two passive filters compared to the standard TDPA. The mathematical necessity of the robot side PC which shows only little dissipation should be evaluated in future work. The passive filters smooth the PC disturbances very effectively but don't critically vanish the force feedback. The OBG clearly improved the coupling behavior by prevention of oscillations at higher delays and through imitation of the desired physical coupling behavior despite delay. In future work, the cross-dimensional artifacts that may appear due to passivity control and the respective compensation methods have to be evaluated.

ACKNOWLEDGMENT

This work was partially funded by the Bavarian Ministry of Economic Affairs, Regional Development and Energy, within the project SMiLE2gether (LABAY102).

REFERENCES

[1] C. Bergenhem, S. Shladover, E. Coelingh, C. Englund, and S. Tsugawa, "Overview of platooning systems," in *Proceedings of the 19th ITS World Congress, Oct 22-26, Vienna, Austria (2012)*, 2012.

[2] T. Muskardin, G. Balmer, S. Wlach, K. Kondak, M. Laiacker, and A. Ollero, "Landing of a fixed-wing uav on a mobile ground vehicle," in *Proceedings of 2016 IEEE International Conference on Robotics and Automation (ICRA)*, 2016, pp. 1237–1242.

[3] G. Niemeyer and J.-J. Slotine, "Stable adaptive teleoperation," *IEEE Journal of oceanic engineering*, vol. 16, no. 1, pp. 152–162, 1991.

[4] M. Franken, S. Stramigioli, S. Misra, C. Secchi, and A. Macchelli, "Bilateral telemanipulation with time delays: A two-layer approach combining passivity and transparency," *Transactions on Robotics*, vol. 27, no. 4, pp. 741–756, 2011.

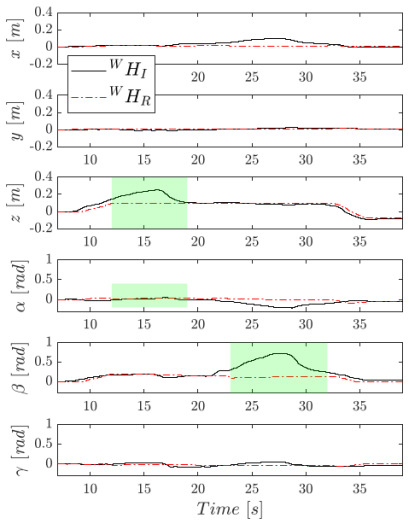

Fig. 17: Pose of Input Device and Robot at 600ms RTD (with OBG)

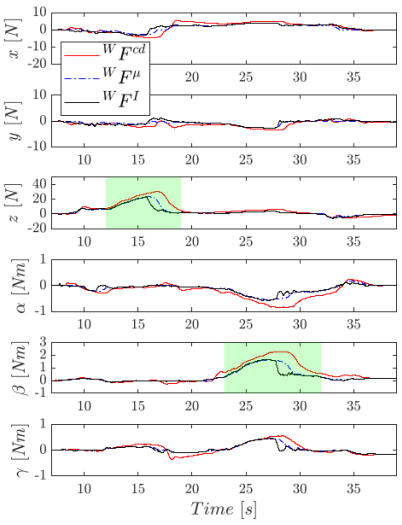

Fig. 18: Wrench on Operator Side at 600ms RTD (with OBG)

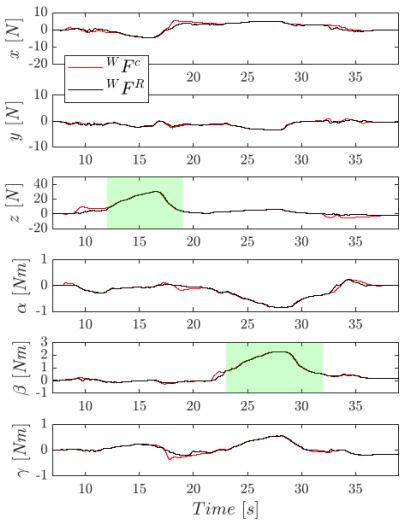

Fig. 19: Wrench on Remote Side at 600ms RTD (with OBG)

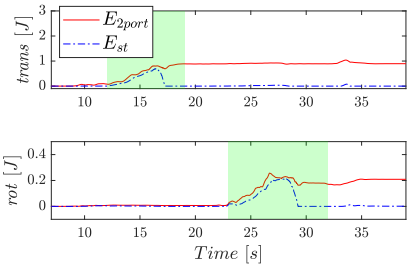

Fig. 20: Passivity Conf. of 2-port at 600ms RTD (with OBG)

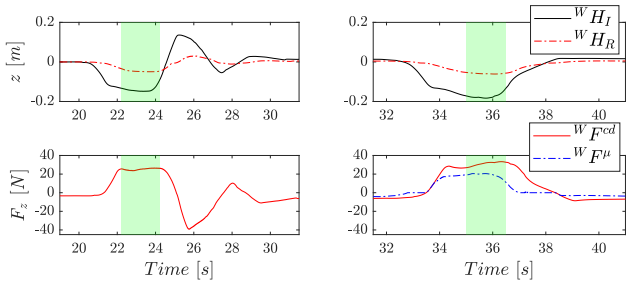

(a) w/o OBG (b) with OBG

Fig. 21: 6DoF Experimental Comparison at 600ms RTD

[5] E. Nuno, L. Basañez, and M. Prada, "Asymptotic stability of teleoperators with variable time-delays," in *Proceedings of 2009 IEEE International Conference on Robotics and Automation (ICRA)*, 2009, pp. 4332–4337.

[6] J.-H. Ryu and C. Preusche, "Stable bilateral control of teleoperators under time-varying communication delay: Time domain passivity approach," in *Proceedings of 2007 IEEE International Conference on Robotics and Automation (ICRA)*, 2007, pp. 3508–3513.

[7] J. Artigas, R. Balachandran, C. Riecke, M. Stelzer, B. Weber, J.-H. Ryu, and A. Albu-Schaeffer, "Kontur-2: force-feedback teleoperation from the international space station," in *Proceedings of 2016 IEEE International Conference on Robotics and Automation (ICRA)*, 2016, pp. 1166–1173.

[8] J. Artigas, R. Balachandran, M. De Stefano, M. Panzirsch, R. Lampariello, A. Albu-Schaeffer, J. Harder, and J. Letschnik, "Teleoperation for on-orbit servicing missions through the astra geostationary satellite," in *Proceedings of 2016 IEEE Aerospace Conference*, 2016, pp. 1–12.

[9] C. Preusche, G. Hirzinger, J.-H. Ryu, and B. Hannaford, "Time domain passivity control for 6 degrees of freedom haptic displays," in *Proceedings of 2003 IEEE/RSJ International Conference on Intelligent Robots and Systems (IROS)*, vol. 3, 2003, pp. 2944–2949.

[10] X. Xu and E. Steinbach, "Elimination of cross-dimensional artifacts in the multi-dof time domain passivity approach for time-delayed teleoperation with haptic feedback," in *Proceedings of 2019 IEEE World Haptics Conference (WHC)*, 2019, pp. 223–228.

[11] M. Panzirsch, H. Singh, T. Krüger, C. Ott, and A. Albu-Schäffer, "Safe Interactions and Kinesthetic Feedback in High Performance Earth-To-Moon Teleoperation," in *Proceedings of 2020 IEEE Aerospace Conference*, 2020, published.

[12] M. Laghi, A. Ajoudani, M. G. Catalano, and A. Bicchi, "Unifying bilateral teleoperation and tele-impedance for enhanced user experience," *The International Journal of Robotics Research*, vol. 39, no. 4, pp. 514–539, 2020.

[13] M. Panzirsch, J.-H. Ryu, and M. Ferre, "Reducing the conservatism of the time domain passivity approach through consideration of energy reflection in delayed coupled network systems," *Mechatronics*, vol. 58, pp. 58–69, 2019.

[14] J.-H. Ryu, J. Artigas, and C. Preusche, "A passive bilateral control scheme for a teleoperator with time-varying communication delay," *Elsevier Journal of Mechatronics*, vol. 20, pp. 812–823, October 2010.

[15] X. Xu, M. Panzirsch, Q. Liu, and E. Steinbach, "Integrating haptic data reduction with energy reflection-based passivity control for time-delayed teleoperation," in *Proceedings of 2020 IEEE Haptics Symposium (HAPTICS)*, 2020, pp. 109–114.

[16] H. Singh, A. Jafari, and J.-H. Ryu, "Enhancing the force transparency of time domain passivity approach: Observer-based gradient controller," in *Proceedings of 2019 IEEE International Conference on Robotics and Automation (ICRA)*, 2019, pp. 1583–1589.

[17] H. Singh, M. Panzirsch, and J.-H. Ryu, "Preserving the physical coupling in teleoperation despite time delay through observer-based gradient control," *IFAC-PapersOnLine*, vol. 52, no. 18, pp. 25–30, 2019.

[18] E. D. Fasse and J. F. Broenink, "A spatial impedance controller for robotic manipulation," *IEEE Transactions on Robotics and Automation*, vol. 13, no. 4, pp. 546–556, 1997.